journal

J. Am. Ceram. Soc., **86** [1] 141–48 (2003)

Scratch Damage in Ceramics: Role of Microstructure

Zong-Han Xie, Mark Hoffman,* Robert J. Moon, and Paul Munroe

School of Materials Science and Engineering, University of New South Wales, NSW 2052, Australia

Yi-Bing Cheng*

School of Physics and Materials Engineering, Monash University, VIC 3800, Australia

Scratch tests were conducted using a standard pyramid indenter against α-SiAlON ceramics with different microstructures: (i) fine equiaxed grains and (ii) large elongated grains. The formation and propagation of cracks were investigated via focused ion-beam milling, with an emphasis on the effect of microstructure on material removal. The fine equiaxed microstructure exhibited high resistance to material removal at low loads, because of its high hardness and homogeneous structure. As the load increased, radial and lateral cracks developed, resulting in large-scale chipping. In contrast, the large elongated microstructure showed a propensity to form microcracks and microabrasion, which is characteristic of partial grain removal, at low loads. With increasing loads, however, the large elongated grains suppressed the propagation of radial and lateral cracks, and, consequently, no large-scale chipping occurred. Implications for material design in abrasive-wear conditions have been discussed.

I. Introduction

Abrasive wear of ceramics is a complex process. To assist in elucidating the mechanisms that control material removal, both static indentation[1–11] and sliding indentation or scratch tests[12–28] have been used to simulate crack formation and abrasion processes.

Several important crack systems in brittle materials, such as radial and lateral cracks, have been investigated systematically by Cook and Pharr[9] using Vickers indentation. "Radial cracks" initiate and grow during the loading segment of an elastic–plastic contact; these cracks emanate from the corners of the indentation. The driving force for the formation of the radial cracks results from the localized loading that is generated by plastic deformation during the indenter contact. "Lateral cracks" form when a material is both loaded and unloaded, depending on the material system. They form beneath the plastic deformation zone at an elastic–plastic contact, are oriented parallel to the surface, and are circular in form. The driving force for the formation of the lateral cracks has been thought to result from the residual stress that results from plastic deformation underneath the indenter contact.[10] "Shallow lateral cracks" are an important variation of the lateral crack. Unlike the classic lateral crack that forms beneath the plastic zone, the shallow lateral crack initiates at the edge of the contact impression and propagates into the material almost parallel to the surface; this type of crack often is bounded by the radial crack.[9]

Many studies have shown that microstructure can have significant influence on crack formation and subsequent material removal;[5–8,17–22,25,26] for a fine-grained microstructure, median/radial and lateral cracks appeared when the material was indented or scratched with a sharp indenter[3,4,13,15,17–22,24,25] (lateral cracks have been assumed to be a major cause for material removal in abrasive processes[13,27]), whereas cone cracks formed when the material was indented or scratched with a blunt (Hertzian) indenter.[11,28] For a coarse-grained microstructure, no median/radial and lateral cracks were observed beyond a critical grain size when the material was scratched with a sharp indenter; instead, subsurface damage took the form of intergranular microcracks and intragrain twin/slip bands.[19–21] Hertzian contact studies also showed that there is a region of maximum shear stress located beneath the contact surface and the propensity for the formation of microcracks increased as the grain size increased.[5–8,11] As a result, coarse-grained microstructures were implied to be a poor design choice for abrasive-wear applications in which microcracking was the controlling process for material removal.[5–7,17–22]

These previous studies have two shortcomings. First, the development and interaction of different crack systems and their influence on material removal in different microstructures have not been explored. Second, although the coarse-grained microstructure has been shown to have a greater potential for microcracking—and, hence, low abrasion resistance—the abrasion behavior of a *nonequiaxed* microstructure has not been demonstrated.

In this study, we use scratch tests to elucidate the effect of equiaxed versus nonequiaxed microstructure on abrasion behavior. Ca α-SiAlON is used as a model polycrystalline system to investigate the formation of different crack systems during scratching and the material removal that results from their interactions. Some implications, based on this investigation, for material design in abrasion applications are also discussed.

II. Experimental Procedure

(1) Materials and Specimen Preparation

Fine equiaxed (noted as "EQ") and large elongated (noted as "EL") α-SiAlON samples were fabricated with the same nominal chemical composition, defined by the formula $Ca_xSi_{12-(m+n)}Al_{m+n}O_nN_{16-n}$, where $x = m/2$, $m = 2.6$, and $n = 1.3$. The processing has been explained in greater detail in an earlier work.[29] These two microstructures are shown in Fig. 1. Some microstructural parameters and mechanical properties are given in Table I.

Disk specimens with a diameter of 25 mm were ground, lapped, then polished consecutively with 15, 6, and 1 μm diamond pastes. Then, the polished specimens were cleaned ultrasonically in acetone for 5 min, rinsed with alcohol and water, and dried at a temperature of 120°C for 10 h.

(2) Scratching and Damage Evaluation

Single-pass scratch tests were conducted using a pin-on-disk-type tribometer (CSEM Instruments, Neuchâtel, Switzerland). The

N. Padture—contributing editor

Manuscript No. 187110. Received March 4, 2002; approved September 20, 2002.
This investigation was supported by an Australian Research Council Large Grant entitled "High Temperature Wear in α-Sialon Ceramics."
*Member, American Ceramic Society.

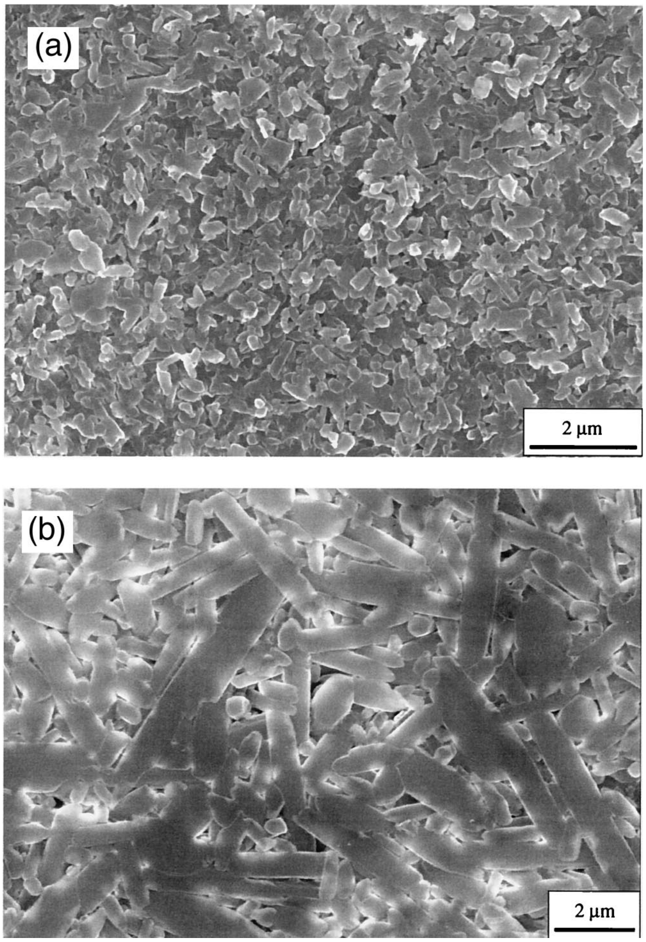

Fig. 1. SEM micrographs of the Ca α-SiAlON microstructures used in this study ((a) fine equiaxed (EQ) and (b) large elongated (EL)). Surfaces etched by molten NaOH.[29]

"pin" was a Vickers pyramid indenter (tip radius of ~1.5 μm), and the sliding direction was parallel to the pyramid diagonal. Testing was performed using a constant velocity of 1 mm/s, in laboratory air with a relative humidity of 50%–60%. Normal loads of 1, 2, 5, and 10 N were used. After scratching, the sample surface was directly gold-coated, without any surface cleaning, thus minimizing any possible disturbance of the surface debris that may have been produced during the testing.

After the gold coating, a focused ion beam (FIB) milling system (Model FEI xP200, FEI Co., Hillsboro, OR) was used to generate cross sections and examine the influence of scratch damage in the two microstructures. The FIB milling system uses a fine (~10 nm) energetic beam of Ga ions that scans over the surface of a specimen. At high beam currents, the beam rapidly sputters sections through the specimen surface and allows a cross section to be prepared. If the beam current is reduced, the secondary electrons emitted from the specimen can be detected and used to generate images similar to conventional scanning electron microscopy (SEM) images. The advantage of this sectioning technique[30] is that micrometer-sized features (microcracks, pores, etc.) that are located within 10 μm of the surface can be captured with minimal damage.

III. Results

Table II provides an explanation of the nomenclature used to describe various features that are visible in the micrographs shown in Figs. 2–8.

(1) Scratching at the Low-Load Region (1 N and 2 N)

The surface and subsurface damage that was caused by scratching on the EQ microstructure at loads of 1 and 2 N is shown in Figs. 2(a) and (b) and 3(a) and (b), respectively. Radial cracks are observed to propagate forward at an angle of ~30° in the scratch direction, relative to the edge of the scratch track. Both the width of the scratch grooves and the length of the radial cracks that intersect the sample surface increased as the scratch load increased. A small amount of scratch debris emerged just to the outside edge of the scratch track at a load of 1 N. More debris could be seen when the load increased to 2 N. The size of the debris is of the order of the grain size and seems to result from fine-grained detachment from the scratch surface. The corresponding cross-sectional views (Figs. 2(b) and 3(b)) show that microcracks formed beneath the scratch groove and are more evident at a load of 2 N, in which a median crack can also be seen.

In contrast, Figs. 2(c) and (d) and Figs. 3(c) and (d) show that no radial cracks appeared in the EL microstructure at scratch loads of 1 and 2 N. Instead, there is a noticeable increase in the amount of scratch debris at the sides of the scratch track, compared with that observed with the EQ microstructure under similar conditions. Further examination of the scratched surface under high magnification revealed more details of the scratched surface, as shown in Fig. 4. The unscratched surface microstructure, which consisted of elongated grains and a grain-boundary glass phase, could be seen to the right of the scratch track (see Section III*(4)*). In contrast, the surface microstructure of the scratched track contained parallel surface cracks that were perpendicular to the scratch direction. A large amount of debris can be seen to the left-hand side of the scratch track; here, the aggregate size is much smaller than the length of the elongated grains, which suggests that the debris was the product of the partial removal of individual elongated grains. In the cross-sectional view (Figs. 2(d) and 3(d)), microcracking can be observed underneath the scratch track; however, no median, lateral, or radial cracks could be seen.

(2) Medium-Load Region (5 N)

The scratching damage in the EQ microstructure at a load of 5 N is shown in Figs. 5(a) and (b). Radial and lateral cracking are observed, as well as chipping, which resulted from the propagation of these two crack systems. Chipping of the material was observed to extend outward from the scratch track with a width of $2c'$, which is approximately twice the width of the scratch track ($2d$). The subsurface view in Fig. 5(b) shows the lateral crack that is present at the edge of the scratch track and extends outward into the material. This type of lateral crack can be considered to be a shallow lateral crack, according to the definition of Cook and Pharr.[9]

In contrast, no chipping is observed in the EL microstructure when the material is scratched under a load of 5 N. Partial grain

Table I. Properties of α-SiAlON EQ and EL Microstructures†

Sample identification	Average grain size (μm)		Aspect ratio	Density (g/cm^3)	Indentation test data at a load of 98 N	
	Diameter	Length			Vickers hardness, H_V (GPa)	Fracture toughness, K_{IC} ($MPa{\cdot}m^{1/2}$)
Fine equiaxed (EQ)	0.35	0.39	1.1	3.19	12.8 ± 0.5	3.7 ± 0.3
Large equiaxed (EL)	0.70	5.04	7.2	3.21	12.0 ± 0.2	7.5 ± 0.3

†From Xie *et al.*[29]

Table II. Nomenclature Used to Describe Features Visible in Figs. 2–8

Symbol	Feature
d	Half-width scratch
c	Length of radial crack from middle of scratch track
c'	Half-width of chipping
D	Scratch debris
m	Microcrack
R	Radial crack
M	Median crack
T	Surface crack
L	Lateral crack
G	α-SiAlON grain
s	Grain-boundary glass phase
➪	Sliding direction of the indenter

removal is still the main form of material loss, as shown in Fig. 5(c). Radial cracks can be seen propagating forward, away from the scratch edge. No obvious increase in the amount of scratch debris is apparent, relative to scratching under lower loads. Meanwhile, the level of subsurface microcracking at the grain boundaries did not change significantly (Fig. 5(d)). Propagation of the microcracks is apparently suppressed by the elongated grains.

(3) High-Load Region (10 N)

During scratching under a load of 10 N, large-scale chipping occurred in the EQ microstructure, as shown in Fig. 6(a). Both the length of the radial cracks and the radius of the lateral cracks increased, which led to the formation of large chips whose average width was ~3 times that of the scratch track. The subsurface view reveals the development of the lateral crack (Fig. 6(b)). A detailed examination on the formation of both radial and lateral cracks was conducted, as shown in Fig. 7. Radial cracks can be seen propagating away from the scratch track and penetrating at angles, which can be either forward or backward to the sliding direction (Fig. 7(b)). The lateral cracks form below the scratch track at two different depths: <1 μm and >2 μm (Fig. 7(b)). The lateral cracks that form within 1 μm of the surface are connected to the parallel surface cracks that are oriented perpendicular to the scratch track. The lateral crack that formed at a location >2 μm below the surface is analogous to those observed in Figs. 5(b) and 6(b) and is believed to originate below the scratch track and extend both along the track and outward from either side of the scratch track.

Chipping was not observed for the EL microstructure; however, severe surface damage was observed along the scratch track, as shown in Fig. 6(c). Broken grains and rod-shaped recesses can be seen from the enlarged view of the scratched surface that is shown in Fig. 8. The subsurface view in Fig. 6(d) shows that discrete microcracks beneath the scratch track seem to coalesce to form lateral cracks. These lateral cracks do not appear to fully develop (i.e., become large and cause chipping). Their propagation may be restricted by crack-growth-resistance behavior that results from the elongated grains.

(4) Etching by Ion Beam

In Fig. 4, the SiAlON grains and grain-boundary glassy phase can be clearly distinguished in the unscratched region to the right of the figure. Such an effect becomes evident after the polished surface has been exposed to an unfocused ion beam at a current of 70 pA for 30–50 s, depending on magnification. This is a very useful technique for microstructure analysis, because SiAlON materials cannot be effectively plasma-etched (because of their crystal structure). Unlike etching with NaOH, the ion-etched surface is essentially flat and gives good contrast between the crystalline and glassy phases.

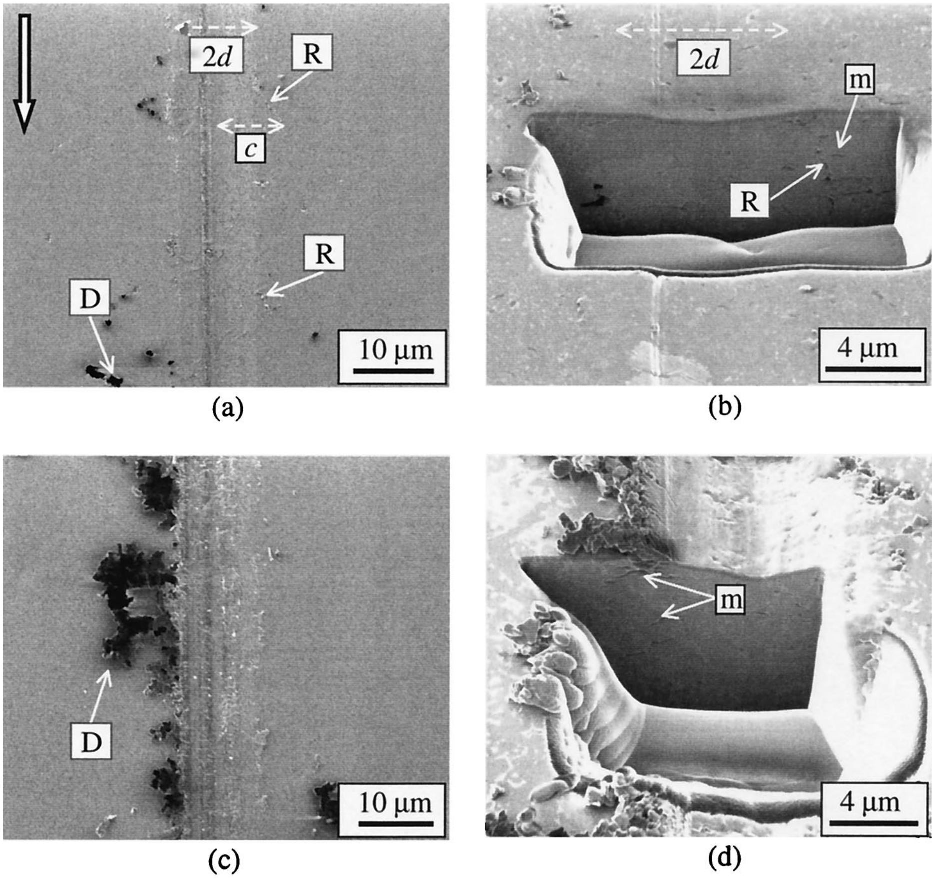

Fig. 2. Damage following scratching at 1 N normal load observed on (a) the surface and (b) the subsurface cross section in the EQ microstructure, and (c) the surface and (d) the subsurface cross section in the EL microstructure.

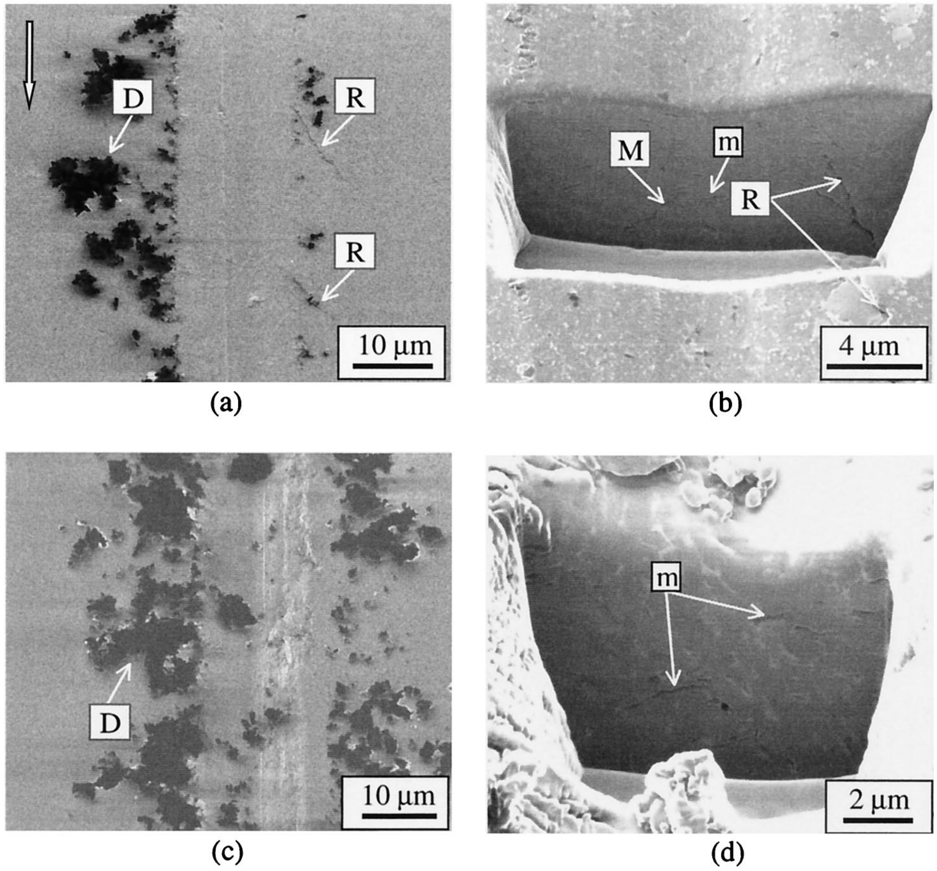

Fig. 3. Damage following scratching at 2 N normal load observed on (a) the surface and (b) the subsurface cross section in the EQ microstructure, and (c) the surface and (d) the subsurface cross section in the EL microstructure.

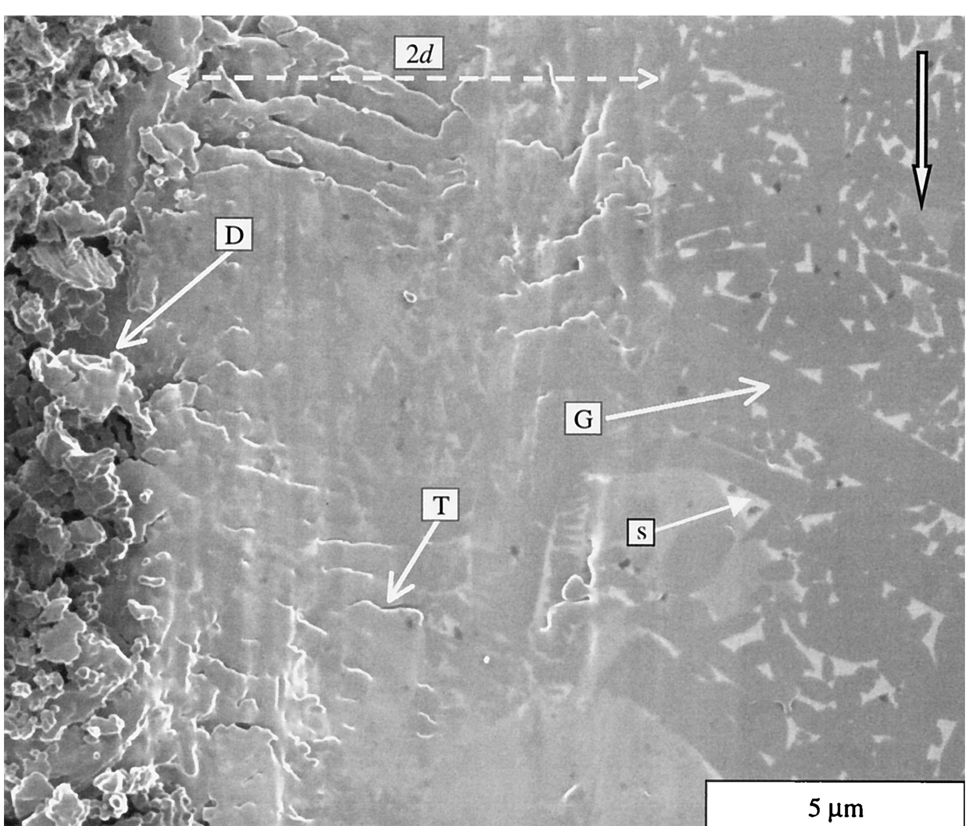

Fig. 4. Detailed image of surface damage in the EL microstructure after scratching under a load of 2 N.

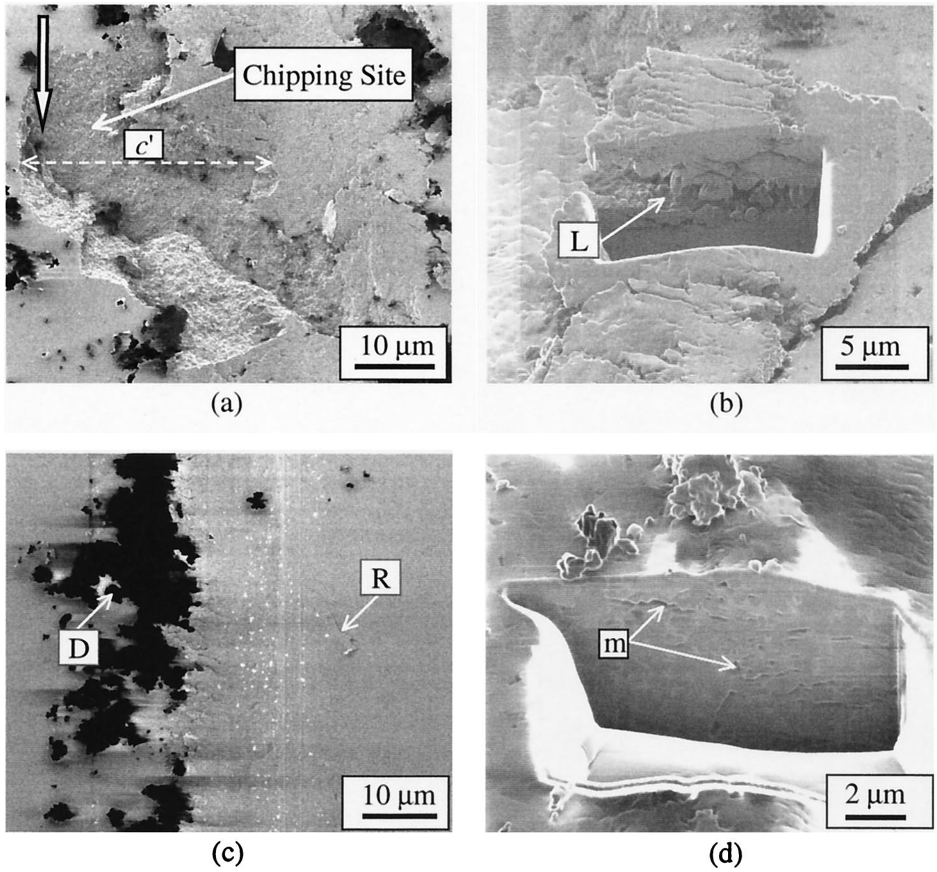

Fig. 5. Damage following scratching at 5 N normal load observed on (a) the surface and (b) the subsurface cross section in the EQ microstructure, and (c) the surface and (d) the subsurface cross section in the EL microstructure.

IV. Discussion

Figures 2–8 demonstrate that microstructure and grain morphology have significant influence on crack formation and subsequent material removal during scratching. Based on the observations in this present work, the scratch damage for the two distinct microstructures will be discussed below.

(1) Crack Formation and Propagation during Scratching

It is important to consider the following factors separately: (i) the initiation of cracks that are up to 1–2 grain sizes in dimension; (ii) the transition of these to the observed radial and lateral cracks; and (iii) the propagation of these to large cracks, which results in chipping. The driving force for crack *initiation* is expected to be the same for both materials, because the chemistry of both EQ and EL microstructures is identical. After crack initiation, both mechanical and microstructural factors become important in determining the formation of the observed radial and lateral cracks and their propagation, as discussed below.

The major difference between static indentation and sliding scratch tests is the presence of tangential force induced by the sliding friction of the indenter. Veldkamp *et al.*[12] investigated the effect of load and speed on crack formation in brittle materials, using a sharp diamond pyramid to scratch on different types of ceramics. According to their work, the minimum tangential force ($F_{t,min}$) for the formation of the observed radial and lateral cracks, during sharp indenter scribing on brittle materials, can be described by

$$F_{t,min} = \chi\left(\frac{K_c^4}{H_S^3}\right) \tag{1}$$

where χ is a constant related to the geometry and orientation of the indenter and the crack type and H_S is the scratching hardness; K_c is the fracture toughness for the formation of the observed radial and lateral cracks. K_c can be expressed as a function of the applied load (P) and the length of the crack (c) that is produced by a sliding sharp indenter:[16]

$$K_c = \xi\left(\frac{P}{c^{3/2}}\right) \tag{2}$$

where ξ is a constant. H_S is usually given as

$$H_S = \frac{4P}{\alpha\pi d^2} \tag{3}$$

where α is a geometrical constant and d is the half width of the scratch groove. Substituting Eqs. (2) and (3) into Eq. (1), the minimum tangential force for the formation of the observed radial and lateral cracks can be rewritten as

$$F_{t,min} = A_n\left(\frac{d}{c}\right)^6 P \tag{4}$$

where A_n is a constant that is related to the geometry of the indenter and the crack type. Figures 2(a) and (c) and Figs. 3(a) and (c) show that the width of the scratch groove in the EQ microstructure is similar to the corresponding scratch in the EL microstructure; thus, both materials have similar scratch hardness, based on Eq. (3). However, although radial cracks were observed in the EQ microstructure at loads of $\geq$1 N, they were not observed in the EL microstructure until the scratch load was 5 N. These observations and Eq. (4) indicate that a greater tangential force is required to form a radial crack of particular length c in the EL microstructure than in the EQ microstructure.

Considering Eq. (1), therefore, it would seem that the reason why a greater tangential force is required to extend microcracks to

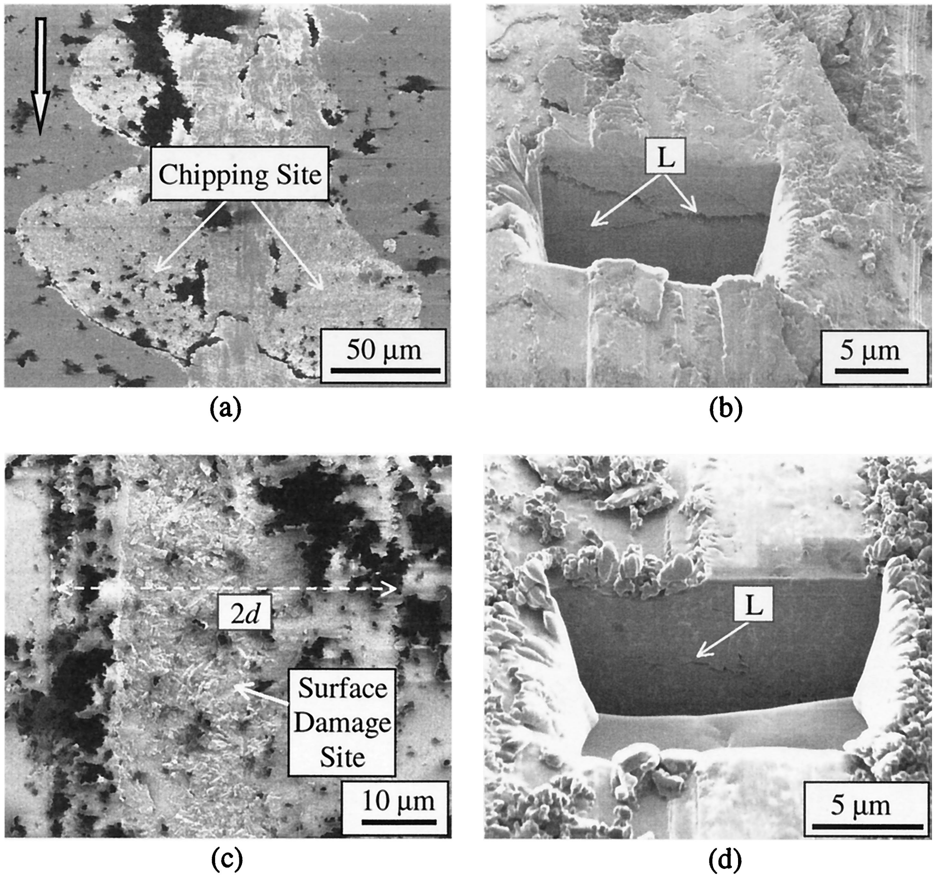

Fig. 6. Damage following scratching at 10 N normal load observed on (a) the surface and (b) the subsurface cross section in the EQ microstructure, and (c) the surface and (d) the subsurface cross section in the EL microstructure.

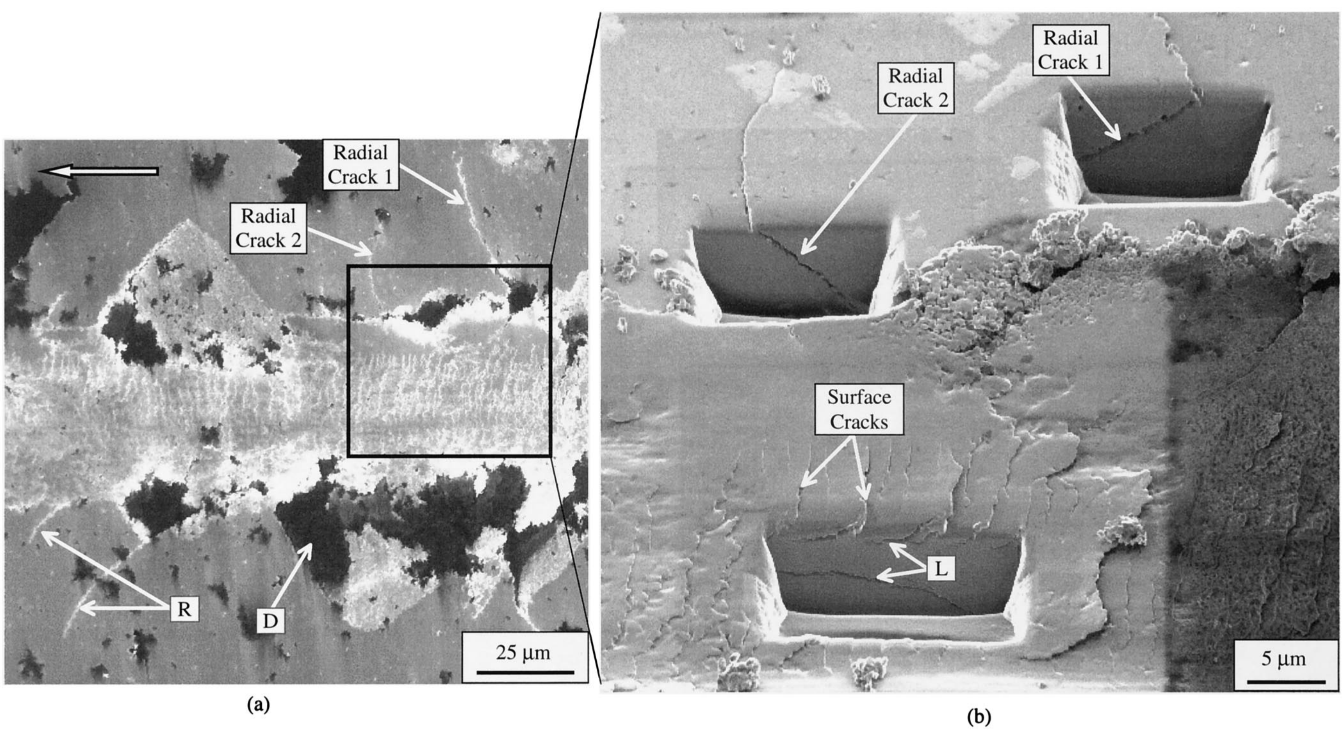

Fig. 7. EQ microstructure scratched under a load of 10 N showing (a) the surface and (b) the subsurface views, showing the formation of radial and lateral cracks, as well as surface cracks. Note that Fig. 7(b) corresponds to the location framed in Fig. 7(a).

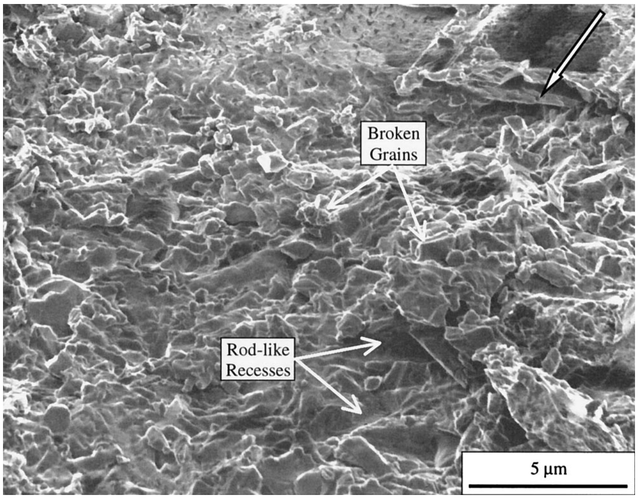

Fig. 8. Detailed image of surface damage in the EL microstructure scratched under a load of 10 N. Note that partial grain removal and individual grain dislodgement occur on the surface.

the observed radial or lateral cracks in the EL microstructure is that the fracture toughness for the *formation* of the observed radial and lateral cracks (K_c) is greater in this material than that for the EQ microstructure. This condition is because both materials demonstrate similar scratch hardness.

Following the formation of the observed radial and lateral cracks, the subsequent propagation of these cracks will be dependent on the fracture toughness for crack *propagation* ($K_{c,\mathrm{prop}}$). Studies have shown that the final crack length following scratch testing can be expressed for radial cracks as[16]

$$c_{\mathrm{R}} = \zeta\left(\frac{P}{K_{c,\mathrm{prop}}}\right)^{2/3} \tag{5}$$

and for lateral cracks as[27]

$$c_{\mathrm{L}} = \kappa\left(\frac{P^{5/8}}{K_{c,\mathrm{prop}}^{1/2}}\right) \tag{6}$$

where both κ and ζ are constants that are dependent on the scratch shape and the elastic–plastic properties of the material. Thus, one can conclude that the fracture toughness $K_{c,\mathrm{prop}}$ is important in determining the magnitude of crack propagation.

As mentioned previously, the driving force for crack initiation should be the same for both materials. Figures 2(b) and (d) in fact show the presence of subsurface microcracks in both materials, following scratching at a load of just 1 N. However, further increases in load reveal that these microcracks do not further develop into radial cracks in the case of the EL microstructure until the scratch load attains a value of 5 N, whereas in the EQ microstructure, the formation of radial cracks is evident at a load of 1 N. Furthermore, although lateral crack propagation is evident at a load of 5 N in the case of the EQ microstructure, lateral cracks are only just visible in the EL microstructure at a load of 10 N and seem to result from microcrack coalescence rather than propagation. In the case of the EQ microstructure at a load of 10 N, radial and lateral cracks have propagated considerably, resulting in extensive chipping, as shown in Fig. 6(a). *R*-curve behavior has been demonstrated in α-SiAlON.[31] Vickers-indentation fracture-toughness measurements, which incorporate the influence of microstructure on crack propagation, revealed that the fracture toughness in the EL microstructure was greater than that of the EQ microstructure, as shown in Table I.[29] Relative to the EQ microstructure, therefore, greater loads are required to cause the microcracks in the EL microstructure to develop into lateral and radial cracks and for these cracks to propagate further.

(2) *Material Removal during Scratching*

For the EQ microstructure, radial cracks formed during scratching under low loads, as shown in Figs. 2(a) and 3(a), and a small amount of material was pushed to the sides of the scratch track due to grain dislodgement; however, no significant material removal occurred. This phenomenon suggests that radial-crack formation alone was not able to cause material removal at low loads. With the increase of load, the extent of radial cracks increased and some intersected each other in the subsurface, as shown in Fig. 7(b), which suggests that this may be one process for chip formation. Meanwhile, lateral cracks developed at two different depths at high load. The lateral cracks that form within 1 μm of the surface interacted with the surface cracks, which led to peeling of the scratch surface (Fig. 7(b)). The lateral cracks that form at a depth of >2 μm into the surface are believed to (i) result in partial removal of the scratch track, as in Fig. 5(a), by extending underneath the scratch track, and (ii) cause large-scale chipping, as in Fig. 6(a), because of their propagation along the sides of the scratch track and intersection with the free surface and/or radial cracks.

Surface cracking that occurred along the scratch track has also been observed in sliding spherical contacts on glass[32] and in pin-on-disk wear studies,[33] in which the large tensile stresses behind the sliding contact initiated surface cracks that subsequently propagate laterally in the near subsurface. Interestingly, however, in this current study and in the wear study,[33] the subsurface cracks propagate in the scratching direction, whereas, in the sliding spherical contact study, the crack propagation was in a direction opposite to the scratching direction.

For the EL microstructure, the debris at the sides of the scratch track demonstrates that material removal occurred; however, no chipping appeared as the load increased. Examination of surface and subsurface damage revealed that the material-removal mechanism is microcracking along the grain boundaries, which leads to partial grain removal at low and medium load (Fig. 4) and a mixture of partial grain removal and individual grain dislodgement at high load (Fig. 8). According to a model proposed by Xu and Jahanmir,[20] in which the process of material removal was assumed to be dominated by microcracking along the grain boundaries, the rate of material removal during scratching for both microstructures at low loads can be calculated as

$$V = \gamma[\psi(\beta l)^{1/2}\sigma_{\mathrm{T}} - K_{c,\mathrm{s}}]\left(\frac{E^{4/5}}{H^{9/5}}\right)P \tag{7}$$

where V represents the volume of material removed per unit scratch length, γ is a constant independent of grain size and load, ψ is the crack-geometry coefficient, the term βl is the initial crack size (assumed to be proportional to the grain length l by a coefficient β), σ_{T} is the tensile stress that is due to the applied load, $K_{c,\mathrm{s}}$ is the short-crack toughness, E is the Young's modulus, and H is the hardness. In this equation, the influences of thermal-expansion anisotropy and damage accumulation are ignored, because the materials tested contained grain-boundary glass phase with low solidification temperature and the test involved just one pass. This equation shows that the microfracture-controlled process of material removal is promoted by increasing the grain length and load and inhibited by increasing the hardness of the material.

This prediction is consistent with the amount of apparent debris that has been observed in this present work at low loads (<5 N), in which a greater rate of material removal by the EL microstructure was observed than by the EQ microstructure. It should also be recognized that the toughness in Eq. (7), $K_{c,\mathrm{s}}$, is not the long-crack toughness ($K_{c,\mathrm{prop}}$) but the *short-crack* toughness, which corresponds to small initial flaws on the order of the grain size. Many studies on the short-crack toughness of ceramics have reported that the fine-grained microstructure exhibits greater short-crack toughness than the large/coarse-grained microstructure[34,35] and attributed this to residual stresses within the microstructure resulting from anisotropy in thermal expansion.[36,37] In this present analysis, the large amount of glassy phase in this α-SiAlON means that there would be limited residual stress, and, hence, the short-crack fracture toughness $K_{c,\mathrm{s}}$ would be expected to be the same for both the EQ and EL microstructures. In addition, similar scratch-track widths mean that the hardness H is the same for both microstructures. For the small volumes of material being considered under a sliding indenter, there is no reason to expect that either of the parameters σ_T or E would be significantly different for the two microstructures. Considering Eq. (7), therefore, differences in the rate of material removal may be attributed to the difference in grain size only.

Some researchers predicted, according to the analysis of short-crack/long-crack toughness effect in ceramic fracture behavior,[5–7,17–22] that the coarse-grained microstructure would exhibit less wear resistance than the fine-grained microstructure in abrasive-wear conditions. This conclusion is correct only when the process of material removal is controlled by microcracking along the grain boundaries.

However, as the load was increased, the advantage of the elongated microstructure (EL) in suppressing the formation and propagation of macrocracking, such as the radial and lateral cracks, became apparent. As a result, large-scale chipping did not occur in the EL microstructure, even at a load of 10 N. Observations of the subsurface structure underneath the scratched track in Fig. 6(d) revealed that no large crack formed, which suggests that the interlocking elongated grains can effectively impede the propagation of the cracks and reduce the severity of surface damage. In the case of the EQ microstructure, the fine equiaxed grains did not lead to grain bridging, and, hence, no impediment to radial and lateral crack propagation existed. This phenomenon resulted in large-scale particle removal in the form of chipping.

(3) Implications for Material Design

Some aspects of material design for abrasive-wear applications can be drawn from this present investigation. For applications in a low-contact-load regime, both the EQ and the EL microstructures exhibit low levels of material removal, with the EQ microstructure exhibiting slightly less material removal. As the contact load in application was increased, the EL microstructure would surpass the EQ microstructure, because of its ability to suppress the propagation of large cracks and subsequent large-scale chipping. However, these implications are notwithstanding the effect of multiple contact-load cycles.

V. Conclusions

The following conclusions can be drawn from the results of this investigation:

(1) The fine, equiaxed grain microstructure (EQ) exhibited good resistance to material removal at low scratch loads, because of its fine grain structure. Radial cracks formed at low loads, but no chipping was induced. As the load was increased, radial cracks propagated. Concurrently, lateral cracks formed and propagated, and large-scale chipping occurred as a result of low long-crack fracture toughness.

(2) The large, elongated grain microstructure (EL) exhibited a slightly greater material-removal behavior than the EQ microstructure at low scratch loads, because of its larger grain size. However, at high load, the formation and propagation of radial and lateral macrocracks was suppressed, and no large-scale chipping occurred.

(3) Both microstructures developed fine subsurface microcracks at low loads.

(4) The EL microstructure may be preferable to the EQ microstructure in abrasive-wear applications This conclusion was due to the interlocking elongated grains in the EL microstructure that caused higher long-crack fracture toughness, which restrained the onset of severe abrasive damage such as chipping.

Acknowledgment

The authors wish to thank Brian Mubaraki for technical support during the tests.

References

[1]B. R. Lawn and M. V. Swain, "Microfracture Beneath Point Indentations in Brittle Solids," *J. Mater. Sci.*, **10,** 113–22 (1975).

[2]B. R. Lawn and R. Wilshaw, "Review of Indentation Fracture: Principles and Applications," *J. Mater. Sci.*, **10,** 1049–81 (1975).

[3]B. R. Lawn and D. B. Marshall, "Indentation Fracture and Strength Degradation in Ceramics"; pp. 205–29 in *Fracture Mechanics of Ceramics*, Vol. 3. Edited by R. C. Bradt, D. P. H. Hassleman, and F. F. Lange. Plenum Press, New York, 1978.

[4]B. R. Lawn, B. J. Hockey, and H. Richter, "Indentation Analysis: Applications in the Strength and Wear of Brittle Materials," *J. Microscopy*, **130** [3] 295–308 (1982).

[5]H. Cai, M. A. S. Kalceff, and B. R. Lawn, "Deformation and Fracture of Mica-Containing Glass-Ceramics at Hertzian Contacts," *J. Mater. Res.*, **9** [3] 762–70 (1994).

[6]F. Guiberteau, N. P. Padture, and B. R. Lawn, "Effect of Grain Size on Hertzian Contact Damage in Alumina," *J. Am. Ceram. Soc.*, **77** [7] 1825–31 (1994).

[7]H. H. K. Xu, L. Wei, N. P. Padture, B. R. Lawn, and R. L. Yeckley, "Effect of Microstructural Coarsening on Hertzian Contact Damage in Silicon Nitride," *J. Mater. Sci.*, **30,** 869–78 (1995).

[8]A. C. Fisher-Cripps and B. R. Lawn, "Indentation Stress–Strain Curves for 'Quasi-Ductile' Ceramics," *Acta Mater.*, **44** [2] 519–27 (1996).

[9]R. F. Cook and G. M. Pharr, "Direct Observation and Analysis of Indentation Cracking in Glasses and Ceramics," *J. Am. Ceram. Soc.*, **73** [4] 787–817 (1990).

[10]D. B. Marshall, B. R. Lawn, and A. G. Evans, "Elastic/Plastic Indentation Damage in Ceramics: The Lateral Crack System," *J. Am. Ceram. Soc.*, **65** [11] 561–66 (1982).

[11]B. R. Lawn, "Indentation of Ceramics with a Sphere: A Century after Hertz," *J. Am. Ceram. Soc.*, **81** [8] 1977–94 (1998).

[12]J. D. B. Veldkamp, N. Hattu, and V. A. C. Snijders, "Crack Formation during Scratching of Brittle Materials"; see Ref. 3, pp. 273–301.

[13]M. V. Swain, "Microfracture about Scratches in Brittle Solids," *Proc. R. Soc. London, A*, **366**, 575–97 (1979).

[14]J. C. Conway and H. P. Kirchner, "The Mechanics of Crack Initiation and Propagation Beneath a Moving Sharp Indentor," *J. Mater. Sci.*, **15,** 2879–83 (1980).

[15]Z. Bi, H. Tokura, and M. Yoshikawa, "Study on Surface Cracking of Alumina Scratched by Single-Point Diamonds," *J. Mater. Sci.*, **23,** 3214–24 (1988).

[16]S. Y. Chen, T. N. Farris, and S. Chandrasekar, "Sliding Microindentation Fracture of Brittle Materials," *Tribol. Trans.*, **34** [2] 161–68 (1991).

[17]H. H. K. Xu and S. Jahanmir, "Scratching and Grinding of a Machinable Glass-Ceramic with Weak Interface and Rising *T*-Curve," *J. Am. Ceram. Soc.*, **78** [2] 497–500 (1995).

[18]H. H. K. Xu and S. Jahanmir, "Effect of Microstructure on Abrasive Machining of Advanced Ceramics," *Ceram. Eng. Sci. Proc.*, **16** [1] 295–314 (1995).

[19]H. H. K. Xu, S. Jahanmir, and Y. Wang, "Effect of Grain Size on Scratch Interactions and Material Removal in Alumina," *J. Am. Ceram. Soc.*, **78** [4] 881–91 (1995).

[20]H. H. K. Xu and S. Jahanmir, "Microfracture and Material Removal in Scratching of Alumina," *J. Mater. Sci.*, **30**, 2235–47 (1995).

[21]H. H. K. Xu and S. Jahanmir, "Effect of Grain Size on Scratch Damage and Hardness of Alumina," *J. Mater. Sci. Lett.*, **14**, 736–39 (1995).

[22]H. H. K. Xu, N. P. Padture, and S. Jahanmir, "Effect of Microstructure on Material-Removal Mechanisms and Damage Tolerance in Abrasive Machining of Silicon Carbide," *J. Am. Ceram. Soc.*, **78** [9] 2443–48 (1995).

[23]Y. Ahn, T. N. Farris, and S. Chandrasekar, "Sliding Microindentation Fracture of Brittle Materials: Role of Elastic Stress Fields," *Mech. Mater.*, **29,** 143–52 (1998).

[24]O. Desa and S. Bahadur, "Material Removal and Subsurface Damage Studies in Dry and Lubricated Single-Point Scratch Tests on Alumina and Silicon Nitride," *Wear*, **225–29**, 1264–75 (1999).

[25]S. K. Lee, R. Tandon, M. J. Readey, and B. R. Lawn, "Scratch Damage in Zirconia Ceramics," *J. Am. Ceram. Soc.*, **83** [6] 1428–32 (2000).

[26]M. G. Gee, "Low Load Multiple Scratch Tests of Ceramics and Hard Metals," *Wear*, **250**, 264–81 (2001).

[27]A. G. Evans and D. B. Marshall, "Wear Mechanisms in Ceramics"; pp. 439–52 in *Fundamentals of Friction and Wear of Materials*. Edited by D. A. Rigney. American Society of Metals, Metals Park, OH, 1981.

[28]B. R. Lawn, "Partial Cone Crack Formation in a Brittle Material Loaded with a Sliding Spherical Indenter," *Proc. R. Soc. London, A*, **299**, 307–16 (1967).

[29]Z.-H. Xie, M. Hoffman, and Y.-B. Cheng, "Microstructural Tailoring and Characterization of a Calcium α-SiAlON Composition," *J. Am. Ceram. Soc.*, **85** [4] 812–18 (2002).

[30]N. Rowlands and P. Munroe, "FIB for the Evaluation of Non-Semiconductor Materials"; pp. 233–41 in *Proceedings of the 31st Annual Technical Meeting of the International Metallographic Society*. Edited by D. O. Northwood, E. Abramovici, M. T. Shehata, and J. Wylie. ASM International, Materials Park, OH, 1998.

[31]M. Zenotchkine, R. Shuba, J. S. Kim, and I-W. Chen, "*R*-Curve Behavior of *In-Situ* Toughened α-SiAlON Ceramics," *J. Am. Ceram. Soc.*, **84** [4] 884–86 (2001).

[32]B. R. Lawn, S. M. Wiederhorn, and D. E. Roberts, "Effect of Sliding Friction Forces on the Strength of Brittle Materials," *J. Mater. Sci.*, **19**, 2561–69 (1984).

[33]T. E. Fisher, M. P. Anderson, and S. Jahanmir, "Influence of Fracture Toughness on the Wear Resistance of Yttria-Doped Zirconium Oxide," *J. Am. Ceram. Soc.*, **72** [2] 252–57 (1989).

[34]L. M. Braun, S. J. Bennison, and B. R. Lawn, "Objective Evaluation of Short-Crack Toughness-Curves Using Indentation Flaws: Case Study on Alumina-Based Ceramics," *J. Am. Ceram. Soc.*, **75** [11] 3049–57 (1992).

[35]N. P. Padture and B. R. Lawn, "Toughness Properties of a Silicon Carbide with *in situ*-Induced Heterogeneous Grain Structure," *J. Am. Ceram. Soc.*, **77** [10] 2518–22 (1994).

[36]P. Chantikul, S. J. Bennison, and B. R. Lawn, "Role of Grain Size in the Strength and *R*-Curve Properties of Alumina," *J. Am. Ceram. Soc.*, **73** [8] 2419–27 (1990).

[37]R. W. Rice, R. C. Pohanka, and W. McDonough, "Effect of Stresses from Thermal Expansion Anisotropy, Phase Transformations and Second Phases on the Strength of Ceramics," *J. Am. Ceram. Soc.*, **63** [11] 703–10 (1980). □